

● *Original Contribution*

ULTRASONIC SPECTRAL PARAMETER CHARACTERIZATION OF APOPTOSIS

M. C. KOLIOS,^{†‡} G. J. CZARNOTA,^{†§} M. LEE,[†] J. W. HUNT^{*‡} and M. D. SHERAR^{*‡§}

[†]Department of Mathematics, Physics and Computer Science, Ryerson University, Toronto, Ontario, Canada;
Departments of [‡]Medical Biophysics and [§]Radiation Oncology, University of Toronto, Toronto, Ontario, Canada;
^{*}Ontario Cancer Institute, Princess Margaret Hospital, Toronto, Ontario, Canada

(Received 28 September 2001; in final form 5 February 2002)

Abstract—Ultrasound (US) spectral analysis methods are used to analyze the radiofrequency (RF) data collected from cell pellets exposed to chemotherapeutics that induce apoptosis and other chemicals that induce nuclear transformations. Calibrated backscatter spectra from regions-of-interest (ROI) were analyzed using linear regression techniques to calculate the spectral slope and midband fit. Two $f/2$ transducers, with operating frequencies of 30 and 34 MHz (relative bandwidths of 93% and 78%, respectively) were used with a custom-made imaging system that enabled the collection of the raw RF data. For apoptotic cells, the spectral slope increased from 0.37 dB/MHz before drug exposure to 0.57 dB/MHz 24 h after, corresponding to a change in effective scatterer radius from 8.7 to 3.2 μm . The midband fit increased in a time-dependent fashion, peaking at 13dB 24 h after exposure. The statistical deviation of the spectral parameters was in close agreement with theoretical predictions. The results provide a framework for using spectral parameter methods to monitor apoptosis in *in vitro* and in *in vivo* systems and are being used to guide the design of system and signal analysis parameters. (E-mail: mkolios@ryerson.ca) © 2002 World Federation for Ultrasound in Medicine & Biology.

Key Words: High frequency ultrasound, Apoptosis, Ultrasound backscatter, Spectral analysis.

INTRODUCTION

Apoptosis, or programmed cell death, has been extensively studied in the past decade and has been recognized to be an integral part of many physiologic processes. It has been thought to play an important role in the response of tumors to cancer therapy (Evan and Vousden 2001; Kallel et al. 1999), other human disease (Stefanec 2000), as well as cellular regulation during embryogenesis (Haanen and Vermes 1996; Meier et al. 2000; van den Eijnde et al. 1997) and the maintenance of homeostasis in developed organisms (Bosman et al. 1996; Schutte and Ramaekers 2000). During apoptosis, the cell self-destructs in an organized and energy-dependent fashion. Striking structural changes occur; the nucleus condenses and then subsequently fragments and the cellular membrane undergoes extensive changes, referred to as blebbing (Hengartner 2000). Although various techniques have been developed to biochemically determine if cells

undergo apoptosis, there are no techniques routinely used today that can noninvasively determine if apoptosis is occurring in cell populations.

Ultrasonic spectral analysis techniques have been used to add information to images generated by conventional ultrasonography (Feleppa et al. 1999; Huisman and Thijssen 1996; Insana et al. 1990; Zagzebski et al. 1993). The spectrum analysis of the radiofrequency (RF) data can provide information on tissue properties such as attenuation and integrated backscatter, as well as more specific information about the scattering sources, such as the effective scatterer size, acoustic impedance and effective concentration. These parameters could provide added information that may aid in the diagnosis of various tissue pathologic states (Huisman et al. 1998; Lizzi et al. 1988; Noritomi et al. 1998; Romijn et al. 1989; Tateishi et al. 1998, 1999). The spectral analysis techniques can be broadly classified as ultrasonic tissue characterization techniques (UTC) and have been extensively investigated for the conventional lower frequency scanners. Few groups, however, have investigated the use of high-frequency ultrasound (US) UTC (Silverman et al. 1986, 1995, 2001; Ursea et al. 1998), partially due to the

Address correspondence to: Dr. Michael C. Kolios, Department of Mathematics, Physics and Computer Science, Ryerson University, 350 Victoria Street, Toronto, Ontario M5B 2K3 Canada. E-mail: mkolios@ryerson.ca

relatively recent development of high-frequency and bandwidth US transducers and the availability of analogue-to-digital cards with sufficient speed for the very high sampling rates required for signal capture. Furthermore, UTC procedures have not been used to investigate the potential for monitoring apoptotic cell populations. The ability of UTC to extract information about changes in the physical characteristics of ultrasonic scatterers makes the technique promising as a method to monitor apoptosis.

We have previously shown that the cellular changes that occur during apoptosis can be detected using high-frequency US (Czarnota et al. 1997, 1999). Individual cells cannot be resolved even at the high frequencies used (30 to 50 MHz); however, changes in the intensity of the backscattered US from cell ensembles can readily be observed. The US backscatter increases as cells undergo apoptosis, thereby increasing the brightness of conventional B-scan images. In this study, we examined if other features of the nonmodified radiofrequency (RF) backscatter signal can be used to detect and measure apoptosis. Specifically, we applied spectral analysis techniques to differentiate apoptotic from healthy cells, and investigated how spectral parameters change with time after apoptosis-inducing drug exposure. The hypothesis that nuclear condensation and fragmentation cause these observed changes in the RF signal was investigated by exposing cells to chemicals that induce nuclear condensation and fragmentation (colchicine and DNase). The spectral analysis results were compared to theoretical predictions and estimates of scatterer sizes were made. The predictions were then compared to histologic images of the cells.

MATERIALS AND METHODS

Biologic samples

Cells were prepared using a cell culture system. For any experimental time point or condition, experiments were completed in duplicate. For each US experiment, approximately 1×10^9 human acute myeloid leukemia cells (AML-5) were grown at 37°C in α -minimal-media from frozen stock samples using 200 mL of media. Cell culture growth was initiated using frozen stock cells. This cell line has a very well characterized apoptotic pathway, and could produce ample cells for our experiments.

Treating the AML cells with the chemotherapeutic agent *cis*-platinum (cisplatin) at 10 μ g/mL induced apoptosis. Cisplatin is a DNA intercalater that causes a p53-dependent apoptosis in this cell line. Cells were treated with the drug for 0, 3, 6, 12, 24 and 48 h. To confirm apoptosis, the 24-h sample was examined using light microscopy, gel electrophoresis showing DNA lad-

dering, and trypan blue staining, confirming that approximately 90% of the cells underwent apoptosis at this time point. Cells were washed in phosphate-buffered saline (PBS) and the preparations were subsequently pelleted in flat bottom cryotubes on a desktop swinging bucket centrifuge. All pellets were the same size with a diameter of 1 cm and a height of 5 mm to 1 cm. Pellets were then immersed in PBS, which acted as the coupling medium for the US imaging. The pellets were kept at room temperature, and experiments were performed within a maximum of 1 h after centrifugation. Cells were arrested in mitosis by treating with the chemotherapeutic agent colchicine at a concentration of 0.1 μ g/mL. This drug inhibits microtubule formation and arrests dividing cells at the G2/M checkpoint of the cell cycle, which corresponds to metaphase of mitosis. In this cell culture system, drug toxicity was visualized at approximately 72 h.

For experiments examining the effects of DNA fragmentation of mitotically-enriched cells on US backscatter, pellets cells were taken and resuspended in 1 mL of PBS. As a control, samples were treated with DNase I (Pharmacia, Peapack, NJ) alone at concentrations of 5413 U/mL and 10,826 U/mL. Samples were also treated as a control with triton X-100 (Sigma, St. Louis, MO) alone at a concentration of 0.1% (w/v). To permeabilize cells and permit DNase I to enter the cells, samples were treated with both DNase I and triton x-100 at the concentrations given above. Digestions proceeded for 15, 30 or 60 min and were terminated by adding EDTA to 500 mM. Effects of DNase I and detergents were assessed histologically.

After the ultrasonic imaging experiments, pellet samples were saved for hematoxylin and eosin (HE) staining by fixing in 10% (w/v) formalin in buffered saline, embedded in paraffin and processed as histologic sections. The morphology of cells at each experimental condition was investigated and analyzed. Light microscopy was carried out using a Zeiss Axioscope 20 (Carl Zeiss, Germany). This microscope was coupled to a SONY CCD camera and recorded digitally on a PC for later analysis of cell morphology.

Ultrasound data acquisition and spectral analysis

The imaging was performed using a custom-built high-frequency US imager (Sherar et al. 1987). Two f/2 transducers were used in these experiments: a 30-MHz 5-mm diameter transducer with a -15 dB bandwidth of approximately 100% (16 to 44 MHz) and a radius of curvature of approximately 9 mm, and a 34-MHz transducer with similar characteristics and a -15 dB bandwidth of 25 MHz (23 to 48 MHz). The use of the two transducers allowed us to verify that the results were not influenced by system transfer functions. A position encoder controlled the transducer motion. For the RF ac-

quisition, transducer coordinates were entered manually under computer control and data were collected at the location of interest. The transducer trigger pulse initiated data acquisition. For each sample examined, image and RF acquisition took 20 min.

In these experiments, 12-bit RF data were acquired along at least 35 independent locations in the cell pellets using an oscilloscope (Lecroy 9362 Model). The scan lines were separated by at least one beamwidth (approximately 55 μm) and were acquired at a sampling rate of 500 MHz. Each stored A-scan was the temporal average of 100 to 200 echoes to decrease noise. Compressed binary RF data were transferred to a workstation for processing. Matlab (Natick, MA; www.mathworks.com) was used to perform signal analysis. The ROI was centered approximately at the transducer focus and was approximately 1 mm in length. The Fourier transform of the ROI was taken using a Hamming apodization function. The power spectrum was obtained by averaging the results from the independent scan lines. This power spectrum was divided by the power spectrum of the echo from a calibration target. A quartz flat was used as the calibration target and the perpendicular reflection off the quartz flat located at the focal point of the transducer was used to derive the power spectrum. This removes system and transducer transfer functions and provides a common reference for data collected with various transducers (Lizzi *et al.* 1983). Linear regression analysis was applied to the calibrated spectral amplitudes (after conversion to dB, labelled dBr). Two parameters from the regression analysis were examined: the spectral slope and the midband fit. The spectral slope is the slope of the linear regression of the calibrated spectrogram and the midband fit is the value of the regression fit at the center frequency over which the spectrum was measured. Assuming a random distribution of scatterers and weak scattering (Born approximation), these parameters can be related to the physical characteristics of the US scatterers (Lizzi *et al.* 1996). The spectral slope is an indicator of effective scatterer shape and size and an increase in slope corresponds to a decrease in effective scatterer size. The midband fit is representative of the US backscatter and depends on the scatterer shape, size, acoustic impedance and concentration. Further details on the technique, as well as theoretical and signal analysis considerations, can be found elsewhere (Feleppa *et al.* 1986; Lizzi *et al.* 1997, 1983, 1988). To generate the theoretical curves used in this paper, equations by Lizzi *et al.* (1996) derived for high-frequency US transducers were used.

RESULTS

After the treatment, the AML cells were centrifuged into pellets of at least 5 mm in height and 1 cm in

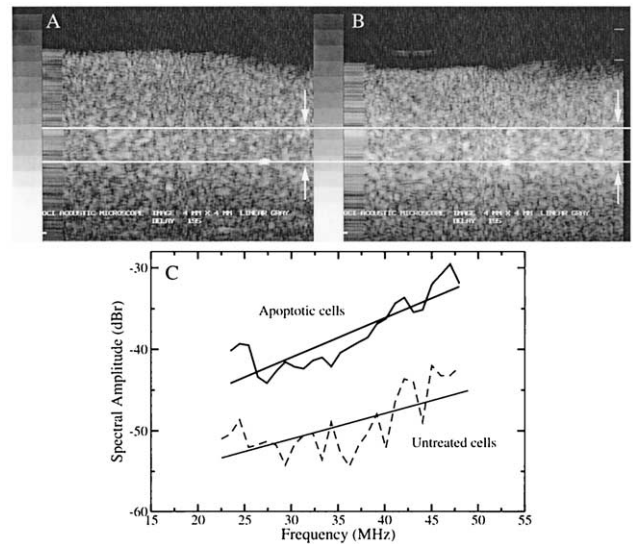


Fig. 1. Ultrasound images of pellets of (a) untreated AML cells and (b) cisplatin-treated AML cells, 24 h after exposure. The pellets are immersed in buffered saline. Horizontal white lines, indicated by arrows, enclose approximate region that RF data were analyzed. US images are 4 mm \times 4 mm. (c) Spectral data from (· · ·) unexposed and (—) cisplatin-exposed AML cell pellets from the ROI shown in (a) and (b).

diameter. Images and RF data were collected for each sample. Exposure of AML cells to cisplatin produced reproducible changes in the US images, RF data and spectral parameters as a function of time after exposure (Figs. 1 and 2a). Figure 1 shows two conventional B-scan images of two pellets: with untreated cells (Fig. 1a) and treated cells (Fig. 1b). The two horizontal lines in the images outline the analysis window that was used in the spectral analysis. Typical results from the signal analysis are shown in Fig. 1c. The normalized power spectrum, derived as outlined in the Methods section, is plotted over the useful bandwidth of the transducer. The data from the apoptotic cell pellets demonstrate an increase in backscatter power (equivalent to an increase in the midband fit) and an increase in slope when compared to the untreated sample.

Raw RF data of US backscatter are plotted in Fig. 2a as a superposition of 30 to 40 independent scans within a pellet. The US backscatter increased as a function of time after cisplatin exposure. Peak-to-peak amplitudes increased by a factor of 3 from normal to apoptotic cell pellets. The backscatter peaked at 24 h after drug exposure and decreased as time progressed. Equivalent changes were seen in the images and have been observed previously (Czarnota *et al.* 1999). Histologic sections from the cell pellets stained using H and E are shown in Fig. 2b. A gradual change in the cell structure is observed, consistent with nuclear condensa-

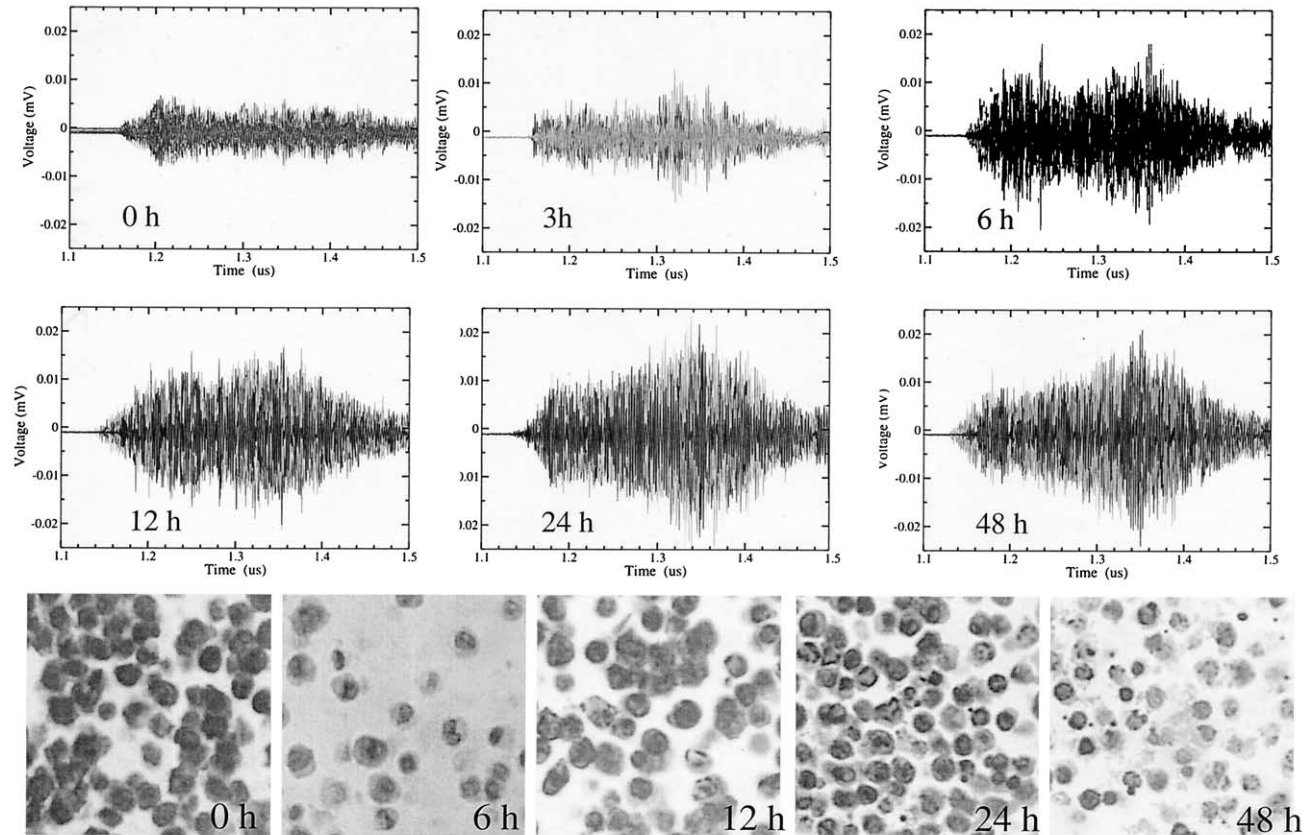


Fig. 2. (a) Superimposed raw backscatter RF data for 30 A-lines using the 34-MHz transducer for AML cells exposed to cisplatin after 0, 3, 6, 12, 24 and 48 h. Backscatter power reaches a peak at approximately 24 h after cisplatin exposure. (b) Representative HE staining of AML cells for several of the time-points mentioned above. In the unexposed AML cells, the nucleus occupies most of the cell and is relatively optically diffuse; with the progression of apoptosis, the nuclear material becomes condensed into small pyknotic bodies composed of condensed fragmented DNA and nucleoprotein.

tion, fragmentation and membrane blebbing seen during apoptosis. The proportion of cells undergoing apoptosis (of any stage) increased with time and, by 24 h, advanced stages of apoptosis were detected histologically for most cells. By 48 h, cellular decay was observed, whereby the entire cell structure disintegrated.

The RF data presented in Fig. 2 were analyzed to extract the spectral slope and midband fit, as described in the Methods section. These parameters are plotted in Fig. 3a. The midband fit ($\cdot\cdot\cdot$) and spectral slope ($—$) are plotted as a function of time after exposure to cisplatin for 6 time-points (0, 3, 6, 12, 24 and 48 h). Both parameters increase with exposure time up to 24 h after cisplatin exposure. The midband fit increased by 13 dB between healthy cells and apoptotic cells. Physical insight to these values may be gained when the values are compared to theoretical predictions. Figure 3b compares the measured values of the spectral slope with theoretical predictions (Lizzi et al. 1997). Superimposed on the

theoretical curve are the experimental slope data presented in Fig. 3a (error bars ± 1 SD). The theory predicts that, for normal cells, the effective scatterer radius was $8.7 \mu\text{m}$ and, for the apoptotic cells (and the 48-h cisplatin exposure time-point), the effective scatterer radius was $3.2 \mu\text{m}$, a reduction by a factor of 2.6. The reduction in effective scatterer radius corresponds well to the reduction in nuclear size as compared to the nuclear fragments seen with the H and E staining; a more rigorous analysis of this observation will follow in the discussion. After the 24 h time-point, which corresponds to the maximal apoptotic response, the spectral slope continued to increase with time while the midband fit decreased.

Nuclear condensation alone can be produced by cell uptake of colchicine. This drug was used to arrest cells at the G2/M cell-cycle checkpoint, which corresponds to metaphase of mitosis. At this point, the cells have condensed nuclear material arranged into mitotic bodies. Cells exposed to colchicine for various time-points were

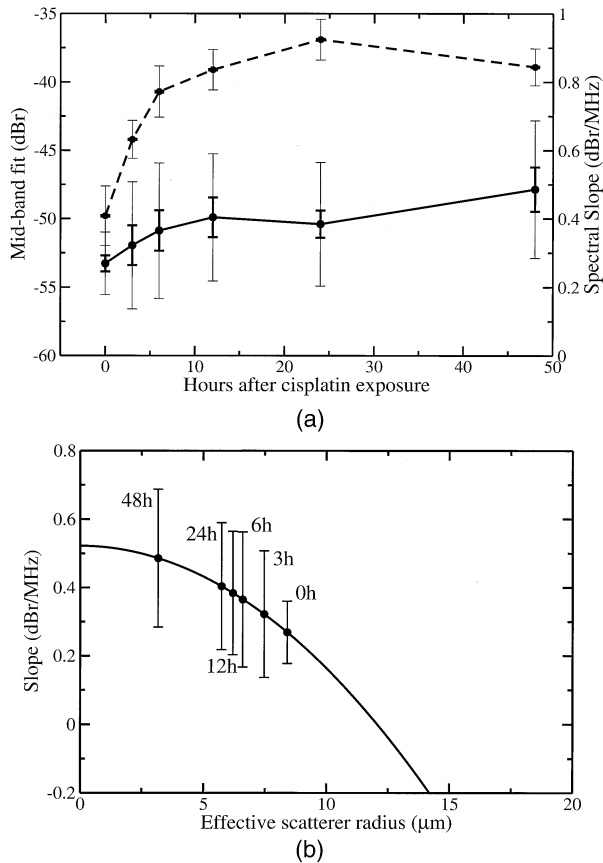


Fig. 3. (a) Plot of the calculated slope (solid curve, right axis) and MBF (intermittent curve) values of the RF data collected in the time-course experiment as a function of time after cisplatin exposure. Thin error bars represent 1 SD and thick errors bars (not visible for the MBF data) the SEM. An increase in both parameters, peaking at 24 h after cisplatin exposure, is observed. (b) Plot of theoretical predictions of spectral slope in dB/MHz as a function of effective scatterer radius (in μm) for the 34-MHz transducer (—) with experimental slope data of the time-course experiment superimposed on the curve (error bars represent 1 SD). A decrease in the effective scatterer radius is observed.

pelleted in a manner similar to the apoptotic cells. In previous experiments, we demonstrated that image brightness of AML pellets exposed to colchicine increased by a factor of 2 to 3, an intermediate level when compared to apoptotic cells (Czarnota *et al.* 1999). The RF data collected in these experiments with the 30- and 34-MHz transducer also confirm this. Table 1 illustrates the effect of adding colchicine to the cell suspension by tabulating the slope and MBF of the RF data for the AML cells exposed to colchicine (after 24 h, and then subsequently exposed to DNase) and the AML cells exposed to cisplatin for comparison. A 7- to 8-dB increase in US intensity was measured when compared to the nontreated AML cells, a result consistent with both

Table 1. The effect of colchicine and colchicine plus DNase (with controls) on the ultrasound spectral parameters of AML cell pellets

	Slope (dBr/MHz) +/- 1 SD	MBF (dBr) +/- 1 SD
AML cells	0.295 +/- 0.181	-45 +/- 1.9
+Colchicine	0.371 +/- 0.194	-37 +/- 1.1
+Cisplatin	0.486 +/- 0.201	-36 +/- 1.3
+Colchicine+DNase+T_30min	0.434 +/- 0.190	-40 +/- 1.1
+Colchicine+DNase+T_60min	0.467 +/- 0.233	-50 +/- 2.6
Theoretical SD	0.176	1.2

Data were collected using the 34-MHz transducer. Errors represent 1SD. Expected value of SD presented in last row (Lizzi *et al.* 1997).

transducers used. The spectral slope increased by an intermediate level when compared to the cisplatin-treated cells. Histologic staining confirms the finding with nuclear condensation occurring at an intermediate level; by 24 h, a maximal cell-cycle arrest was visualized histologically and indicated by cytometric analysis to be approximately 30% (the maximal mitotic fraction that the cell line exhibits in response to colchicine). We have postulated that the initial nuclear condensation was responsible for some of the increase in backscatter observed in cells undergoing apoptosis.

To determine how the spectral parameters changed when colchicine-treated cells were exposed to a DNase, thereby reversing the effects of DNA condensation, the mitotic cells were treated with an excess of DNase I with the presence of a permeabilizing detergent at the time point of maximal mitotic arrest (approximately 24 h). Controls were included to ensure the changes observed were a result of the DNase activity and not the activity of the detergent. The data were collected with the 34-MHz

Table 2. The effect of DNase on the spectral parameters of AML cell pellets exposed to colchicine as a function of exposure time to DNase

	Slope (dBr/MHz) +/- 1 SD	MBF (dBr) +/- 1 SD
AML cells	0.366 +/- 0.163	-56 +/- 1.4
+Colchicine	0.450 +/- 0.164	-50 +/- 2.4
+Colchicine+DNase+T_15min	0.473 +/- 0.185	-53 +/- 3.1
+Colchicine+DNase+T_30min	0.526 +/- 0.166	-52 +/- 3.0
+Colchicine+DNase+T_60min	0.528 +/- 0.222	-56 +/- 3.3
+ Cisplatin	0.572 +/- 0.093	-47 +/- 2.1
Theoretical SD	0.131	1.1

Data were collected with the 30 MHz transducer. Triton was added in the DNase experiments to ensure DNase transport to the nucleus. Spectral parameters derived from exposure to cisplatin added as a comparator. Errors represent 1SD. Expected value of SD presented in last row (Lizzi *et al.* 1997).

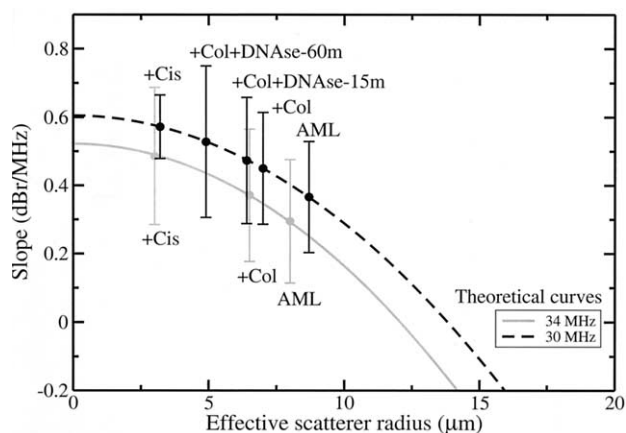


Fig. 4. Plot of spectral slope theoretical predictions as a function of effective scatterer radius (in μm) for the 34-MHz (solid curve) and 30-MHz (intermittent curve) transducer with experimental slope data from the colchicine and DNase experiments superimposed on the curves. Error bars represent 1 SD.

transducer and are presented in Table 2. Using three different DNase time exposures, 15, 30, and 60 min, the US backscatter was found to decrease toward that of the normal cells, and the spectral slope increased with exposure time. The decrease in the midband fit, corresponding to a decrease in backscatter, is consistent with our previous findings. The midband fit was reduced by 8 to 10 dB and the spectral slope further increased, consistent with the decrease in effective scatterer size.

In Fig. 4, the spectral slope calculated in Tables 1 and 2 are superimposed on theoretical curves of spectral slope vs. effective scatterer size, as in Fig. 3b. The two curves on the plot are derived theoretically and based on the physical characteristics of the 30- and 34-MHz transducers. Superimposed on the curves are a subset of the data points from Tables 1 and 2. The spectral slope decreased in all experiments involving nuclear transformations. Cells exposed to cisplatin were predicted to have the smallest effective scatterer radius, and colchicine-exposed cells had an intermediate slope (when compared to the unexposed and cisplatin-treated cells), which decreased upon exposure to DNase. In Fig. 4, the data collected using the 30-MHz transducer for various DNase exposure times are also presented. The spectral slope increased with DNase exposure time and the MBF decreased (Table 2). Despite the fact that the experiments were done with different batches of AML cells, on different dates and using two different transducers to collect the RF data, predicted effective scatterer radii were in general in agreement based on the measured slope data. Furthermore, the SD of the measured spectral properties is in close agreement with theoretical values (Lizzi et al. 1997). The differences in absolute values for the mid-

band fit are due to the different efficiencies of the transducers. The relative increase in the midband fit, however, is consistent for both transducers.

DISCUSSION

We have previously shown that high-frequency US imaging can be used to detect processes that result in large changes in nuclear structure, such as programmed cell death or apoptosis (Czarnota et al. 1997, 1999). This paper explores the use of spectral parameters based on RF US backscatter data for the detection and measurement of apoptosis and other processes that result in changes in nuclear structure. RF data from cells that were exposed to chemotherapeutics that induce specific structural changes to the cell nucleus, amongst other targets, were analyzed. Spectral parameters were derived that were then used in a theoretical model to predict features of the scatterer microstructure and organization. Specifically, the spectral slope and midband fit were used to characterize the signals. The theoretical model (Lizzi et al. 1983) assumes that the scatterers are small and weak (Born approximation), isotropic (in this case spherical) and randomly positioned in space. The analysis region is assumed to be near the focal plane of the focused transducer with negligible attenuation due to intervening tissue. Furthermore, it is assumed that the window used in the analysis is longer in time than the duration of the echo from an individual scatterer. It is known that scattering from tissues is weak and it is reasonable to assume that scattering structures are smaller than the wavelength of the interrogating US (40 to 50 μm in this case). Therefore, the weakest assumptions are those of negligible intervening attenuation and random scatterer distribution.

The spectral slope of the backscatter signal increased in all experiments involving nuclear structure manipulation (condensation and fragmentation), a result consistent with the histologic and biochemical analysis demonstrating smaller condensed nuclear structures. The spectral slope is affected by tissue attenuation and is related to the correlation dimensions (effective size or radius) of the tissue scatterers (Lizzi et al. 1988). Assuming spherical scatterers and minimal attenuation before the analysis region, the increase in spectral slope from 0.36 dBr/MHz to 0.57 dBr/MHz (normal vs. apoptotic, 30 MHz transducer) corresponds to a decrease in the effective scatterer radius from 8.7 to 3.2 μm . The diameter of the unexposed cell nucleus was, on average, 5 μm . Therefore, the calculated effective scatterer diameter of 17.4 μm overestimates the nuclear diameter by a factor of 3.5. Apoptotic cells produce nuclear fragments with diameters of 1 to 2 μm (Czarnota et al. 1999). The relative decrease in scatterer size estimated from the

spectral analysis corresponds well to the changes in nuclear diameter seen histologically. However, the source of backscatter remains elusive. It is known that changes in acoustic impedance are responsible for ultrasonic backscatter. At the subcellular scales of interest here, variations of acoustic impedance are unknown. We are currently in the process of measuring the ultrasonic properties of isolated cell components to help identify the primary scattering centers of the cell. The evidence presented to date (Czarnota *et al.* 1999; Kolios *et al.* 1999) and in this paper, as well as experiments in progress on isolated nuclei of AML cells, indicate that the scattering centers are in the cell nucleus.

The midband fit is a measure of the US backscatter. It is dependent on the attenuation as well as the effective scatterer size, concentration and the acoustic impedance change between the acoustic scatterer and the surrounding medium. Changes in the midband fit, closely related to backscatter, followed the anticipated pattern based on our previous work (Czarnota *et al.* 1999): an increase with apoptosis and condensation and a decrease with cell exposure to DNase. Interestingly, exposure of the colchicine-treated cells to DNase decreased the US backscatter to pre-exposure levels, indicative of dissolution of the condensed nuclear material. The spectral slope, however, increased instead of decreasing to the pre-exposure levels, suggesting that smaller effective scatterer sizes gave rise to the signal. This can also be seen in the histology because the nuclear material is not condensed. As in the case with spectral slopes, theoretical values can be derived for the midband fit and compared to the experimental values. However, the concentration of scatterers must be known as well as their acoustic impedance mismatch with the surrounding medium. Because the nature of the scatterers is unknown, these values cannot be obtained. Due to the number of unknown parameters involved, quantitative analysis of the midband fit was not performed. After our experiments with isolated cell components are completed, the data could be revisited to make quantitative statements about model applicability and parameter estimation.

If the hypothesis that the cell nucleus accounts for most of the backscatter is true, then we can qualitatively elucidate the changes in US backscatter seen in the experiments. The process of nuclear condensation takes place in the early stages of apoptosis as in mitosis, and condenses chromosomes from forms distributed roughly throughout the whole of the cells' nucleus to the more compact chromosomes found in apoptotic and mitotic cells. These compact chromosomes are much smaller than the interrogating US wavelength (44 to 50 μm) and, therefore, can be treated as Rayleigh scatterers preferentially scattering the higher frequency components of the pulse. As the effective scatterer radius in Figs. 3b and 4

approaches 0, the maximum value of slope is reached, and it can be shown that this corresponds to Rayleigh scattering (*i.e.*, a fourth power dependence on frequency of the US backscatter power). The interpretation of the increased backscatter (or equivalently midband fit) is more complex. The increase can be due to the increase in nuclear scattering cross-section, a result of the nuclear condensation, or due to the increase in randomization of the scatterer distribution due to the nuclear condensation and fragmentation. We are aggressively pursuing both theoretical and experimental avenues to answer this question. Preliminary experiments seem to indicate that both play a role.

Spectral analysis, as applied to high-frequency and bandwidth transducers used in these experiments, poses special challenges when compared with the conventional lower frequency spectral methods. Because the focal length of the transducers is small, it must be ensured that axial variations in the intensity are avoided in the ROI. Therefore, the analysis window was enclosed within the focal region of both transducers used, and centered on the focal point of the transducer. For future experiments where such precision in probe placement cannot be achieved, we are investigating the use of scattering phantoms as a calibration technique to provide more accurate correction mechanisms for any depth of interest (Huisman *et al.* 1998; Oosterveld *et al.* 1991; Thijssen *et al.* 1991).

The spectral parameters presented were not corrected for attenuation of intervening tissue. The measured attenuation coefficients for normal and apoptotic cells were 0.077 dB/MHz/mm and 0.072 dB/MHz/mm, respectively (Warrington *et al.*, unpublished observations). Furthermore, either 0.75 mm or 1 mm of tissue intervened before the analysis region. Therefore, the spectral slope and midband fit values presented are likely underestimated. Correction factors can be calculated based on the above measured coefficients and knowledge of the location and length of the analysis windows used. For both transducers, the analysis windows were 1 μs and, assuming the speed of sound 1.5 mm/ μs , a window length of 0.75 mm. The length of the intervening tissue (from the pellet surface to the ROI) was a maximum of approximately 0.75 mm for the 30-MHz transducer and 1 mm for the 34-MHz transducer. Therefore, due to the effect of the intervening tissue, the tabulated slopes were reduced due to attenuation by a maximum of approximately 0.058 dB/MHz (for the 30-MHz transducer) and 0.077 dB/MHz (for the 35-MHz transducer). Size predictions become more accurate by applying this correction. For example, based on the slopes of Table 2 (Fig. 4), the effective scatterer size is 8.8 μm for the unexposed AML cells and 3.5 μm for the cisplatin-treated cells 48 h after exposure. Applying the correction, the

radii are 7.8 μm and 1.8 μm , respectively, better reflecting scatterer sizes measured histologically. Caution must be used in the interpretation of the results because the wavelength (40 to 50 μm) is greater than the scatterers. Furthermore, as alluded to above, it is not known what structures are the primary determinants of US backscatter in the cell pellet system. These corrections were not applied to all samples presented in the figures and tables because attenuation was not measured for all experimental conditions. Visual inspection of the RF lines, however, indicates that the values likely do not significantly change between samples.

An examination of the statistics of the spectral parameters reveals that the standard deviation values obtained are in good agreement with expected values (Tables 1 and 2, based on theoretical analysis (Lizzi et al. 1997)). Because the cell pellets (and tissues) exhibit stochastic scattering structures (in terms of size, shape and physical properties), the calculated parameters form statistical estimates of some true ensemble average characteristic of the tissue within the ROI (Lizzi et al. 1983). The statistics of each spectral parameter can be compared to theoretical probability density functions (from which the SDs of Tables 1 and 2 were calculated), which can then be used to evaluate the precision of estimating scatterer properties (Huisman and Thijssen 1996; Lizzi et al. 1997). Moreover, this would help to separate measurement variance due to the method from the inherent tissue property variance. Deviations from the theoretical values can be associated with local heterogeneities or with the presence of coherent scatterers, since it is assumed in the theoretical model that the scatterers are distributed randomly in space. Because it is not known what the scatterers are, their spatial distribution cannot be determined.

This report presents the results of applying signal analysis methods to detect apoptosis in an *in vitro* model using high-frequency US. We would like to apply the same methodology in tissues to monitor the progression of apoptosis, either in experimental animal models or to monitor the natural progression of tissues during development. Furthermore, we are interested in using this method to monitor the response to cancer therapy: Lymphomas respond by programmed cell death to steroid treatment, melanomas often exhibit apoptosis in response to experimental therapies, and basal cell carcinomas also often exhibit a high apoptotic response to treatment protocols. One may envisage the ultrasound imaging and spectroscopy method being used to evaluate the effects of treatment regimens *in vivo*. It is anticipated that the response of tumors to such therapies to be more complex. Furthermore, other tissue structures would scatter the US, and their effect on the analysis presented is unknown. The pellets used in these experiments represent a

simple system to monitor tissue changes at the cellular level that occur *in vivo*; other tissue structures and their changes during the treatment may have a significant effect on the US backscatter (Hall et al. 2000).

We have currently started animal studies to ascertain these effects, aided with a commercial version of the US prototype (VS40B—VisualSonics Inc, Toronto, Ontario, Canada) that was used in these studies that can digitally acquire the RF data from an ROI selected by the user guided by the conventional B-scan image. The US imager not only automates the data collection process, but also allows rapid RF data acquisition required when there is motion of the subject. Finally, while at these high frequencies, the approach would be limited to subcutaneous ROIs, developments in transducer technology may soon permit transducers to be mounted on catheters that can be used to image deep-seated tumors in a minimally invasive manner. Therefore, this method can be used to complement the image data generated and provide useful diagnostic information.

Acknowledgements—The Medical Research Council of Canada (now Canadian Institute of Health Research) and the Natural Science and Engineering Council of Canada (NSERC) supported this work. The authors acknowledge the essential contributions of Dr. Stuart Foster and the technical assistance and advice of Arthur Worthington and Kasia Harasiewicz.

REFERENCES

- Bosman FT, Visser BC, van Oeveren J. Apoptosis: Pathophysiology of programmed cell death. *Pathol Res Pract* 1996;192(7):676–683.
- Czarnota GJ, Kolios MC, Abraham J, et al. Ultrasound imaging of apoptosis: High-resolution non-invasive monitoring of programmed cell death in vitro, in situ and in vivo. *Br J Cancer* 1999;81(3):520–527.
- Czarnota GJ, Kolios MC, Vaziri H, et al. Ultrasonic biomicroscopy of viable, dead and apoptotic cells. *Ultrasound Med Biol* 1997;23(6):961–965.
- Evan GI, Vousden KH. Proliferation, cell cycle and apoptosis in cancer. *Nature* 2001;411(6835):342–348.
- Feleppa EJ, Fair WR, Tsai H, et al. Progress in two-dimensional and three-dimensional ultrasonic tissue-type imaging of the prostate based on spectrum analysis and nonlinear classifiers. *Mol Urol* 1999;3(3):303–310.
- Feleppa EJ, Lizzi FL, Coleman DJ, Yaremko MM. Diagnostic spectrum analysis in ophthalmology: A physical perspective. *Ultrasound Med Biol* 1986;12(8):623–631.
- Haanen C, Vermes I. Apoptosis: Programmed cell death in fetal development. *Eur J Obstet Gynecol Reprod Biol* 1996;64(1):129–133.
- Hall CS, Nguyen CT, Scott MJ, Lanza GM, Wickline SA. Delineation of the extracellular determinants of ultrasonic scattering from elastic arteries. *Ultrasound Med Biol* 2000;26(4):613–620.
- Hengartner MO. The biochemistry of apoptosis. *Nature* 2000;407(6805):770–776.
- Huisman HJ, Thijssen JM. Precision and accuracy of acoustospectrographic parameters. *Ultrasound Med Biol* 1996;22(7):855–871.
- Huisman HJ, Thijssen JM, Wagener DJ, Rosenbusch GJ. Quantitative ultrasonic analysis of liver metastases. *Ultrasound Med Biol* 1998;24(1):67–77.
- Insana MF, Wagner RF, Brown DG, Hall TJ. Describing small-scale structure in random media using pulse-echo ultrasound. *J Acoust Soc Am* 1990;87(1):179–192.
- Kallel F, Stafford RJ, Price RE, et al. The feasibility of elastographic

- visualization of HIFU-induced thermal lesions in soft tissues. Image-guided high-intensity focused ultrasound. *Ultrasound Med Biol* 1999;25(4):641–647.
- Kolios MC, Czarnota GJ, Lee M, Hunt JW, Sherar MD. Ultrasonic spectrum analysis of apoptotic cell populations. *FASEB J* 1999;13:A1435.
- Lizzi FL, Astor M, Feleppa EJ, Shao M, Kalisz A. Statistical framework for ultrasonic spectral parameter imaging. *Ultrasound Med Biol* 1997;23(9):1371–1382.
- Lizzi FL, Astor M, Kalisz A, et al. Ultrasound spectrum analysis for different scatter morphologies: theory and very-high frequency results. Piscataway, NJ: IEEE 1996; pp 1155–1159.
- Lizzi FL, Greenebaum M, Feleppa EJ, Elbaum M, Coleman DJ. Theoretical framework for spectrum analysis in ultrasonic tissue characterization. *J Acoust Soc Am* 1983;73(4):1366–1373.
- Lizzi FL, King DL, Rorke MC, Hui J, Ostromogilsky M, Yaremko MM, Feleppa EJ, Wai P. Comparison of theoretical scattering results and ultrasonic data from clinical liver examinations. *Ultrasound Med Biol* 1988;14(5):377–385.
- Meier P, Finch A, Evan G. Apoptosis in development. *Nature* 2000;407(6805):796–801.
- Noritomi T, Machi J, Feleppa EJ, Yanagihara E, Shirouzu K. In vitro investigation of lymph node metastasis of colorectal cancer using ultrasonic spectral parameters. *Ultrasound Med Biol* 1998;24(2):235–243.
- Oosterveld BJ, Thijssen JM, Hartman PC, Romijn RL, Rosenbusch GJ. Ultrasound attenuation and texture analysis of diffuse liver disease: Methods and preliminary results. *Phys Med Biol* 1991;36(8):1039–1064.
- Romijn RL, Thijssen JM, van Delft JL, et al. In vivo ultrasound backscattering estimation for tumour diagnosis: An animal study. *Ultrasound Med Biol* 1989;15(5):471–479.
- Schutte B, Ramaekers FC. Molecular switches that govern the balance between proliferation and apoptosis. *Prog Cell Cycle Res* 2000;4:207–217.
- Sherar MD, Noss MB, Foster FS. Ultrasound backscatter microscopy images the internal structure of living tumour spheroids. *Nature* 1987;330(6147):493–495.
- Silverman RH, Coleman DJ, Lizzi FL, et al. Ultrasonic tissue characterization and histopathology in tumor xenografts following ultrasonically induced hyperthermia. *Ultrasound Med Biol* 1986;12(8):639–645.
- Silverman RH, Lizzi FL, Ursea BG, et al. High-resolution ultrasonic imaging and characterization of the ciliary body. *Invest Ophthalmol Vis Sci* 2001;42(5):885–894.
- Silverman RH, Rondeau MJ, Lizzi FL, Coleman DJ. Three-dimensional high-frequency ultrasonic parameter imaging of anterior segment pathology. *Ophthalmology* 1995;102(5):837–843.
- Stefanec T. Endothelial apoptosis: Could it have a role in the pathogenesis and treatment of disease? *Chest* 2000;117(3):841–854.
- Tateishi T, Machi J, Feleppa EJ, et al. In vitro B-mode ultrasonographic criteria for diagnosing axillary lymph node metastasis of breast cancer. *J Ultrasound Med* 1999;18(5):349–356.
- Tateishi T, Machi J, Feleppa E. J, et al. In vitro diagnosis of axillary lymph node metastases in breast cancer by spectrum analysis of radio frequency echo signals. *Ultrasound Med Biol* 1998;24(8):1151–1159.
- Thijssen JM, Verbeek AM, Romijn RL, de Wolff-Rouendaal D, Oosterhuis JA. Echographic differentiation of histological types of intraocular melanoma. *Ultrasound Med Biol* 1991;17(2):127–138.
- Ursea R, Coleman DJ, Silverman RH, Lizzi FL, Daly SM, Harrison W. Correlation of high-frequency ultrasound backscatter with tumor microstructure in iris melanoma. *Ophthalmology* 1998;105(5):906–912.
- van den Eijnde SM, Luijsterburg AJ, Boshart L, et al. In situ detection of apoptosis during embryogenesis with annexin V: From whole mount to ultrastructure. *Cytometry* 1997;29(4):313–320.
- Zagzebski JA, Lu ZF, Yao LX. Quantitative ultrasound imaging: In vivo results in normal liver. *Ultrasound Imaging* 1993;15(4):335–351.